Mechanism-Based Inhibition of Sir2 Deacetylases by Thioacetyl-Lysine Peptide †

ARTICLE *in* BIOCHEMISTRY · JANUARY 2008

Impact Factor: 3.02 · DOI: 10.1021/bi7013294 · Source: PubMed

2 AUTHORS, INCLUDING:

Brian Christopher Smith
Medical College of Wisconsin
24 PUBLICATIONS **1,604** CITATIONS

Mechanism-Based Inhibition of Sir2 Deacetylases by Thioacetyl-Lysine Peptide[†]

Brian C. Smith[‡] and John M. Denu*[,§]

Departments of Chemistry and Biomolecular Chemistry, University of Wisconsin, Madison, Wisconsin 53706

Received July 5, 2007; Revised Manuscript Received September 5, 2007

ABSTRACT: Sir2 protein deacetylases (or sirtuins) catalyze NAD^+-dependent conversion of ϵ-amino-acetylated lysine residues to deacetylated lysine, nicotinamide, and 2′-*O*-acetyl-ADP-ribose. Small-molecule modulation of sirtuin activity might treat age-associated diseases, such as type II diabetes, obesity, and neurodegenerative disorders. Here, we have evaluated the mechanisms of sirtuin inhibition of histone peptides containing thioacetyl or mono-, di-, and trifluoroacetyl groups at the ϵ-amino of lysine. Although all substituted peptides yielded inhibition of the deacetylation reaction, the thioacetyl-lysine peptide exhibited exceptionally potent inhibition of sirtuins Sirt1, Sirt2, Sirt3, and Hst2. Using Hst2 as a representative sirtuin, the trifluoroacetyl-lysine peptide displayed competitive inhibition with acetyl-lysine substrate and yielded an inhibition constant (K_{is}) of 4.8 μM, similar to its K_d value of 3.3 μM. In contrast, inhibition by thioacetyl-lysine peptide yielded an inhibition constant (K_{is}) of 0.017 μM, 280-fold lower than its K_d value of 4.7 μM. Examination of thioacetyl-lysine peptide as an alternative sirtuin substrate revealed conserved production of deacetylated peptide and 1′-SH-2′-*O*-acetyl-ADP-ribose. Pre-steady-state and steady-state analysis of the thioacetyl-lysine peptide showed rapid nicotinamide formation (4.5 s^{-1}) but slow overall turnover (0.0024 s^{-1}), indicating that the reaction stalled at an intermediate after nicotinamide formation. Mass spectral analysis yielded a novel species (*m*/*z* 1754.3) that is consistent with an ADP-ribose-peptidyl adduct (1′-*S*-alkylamidate) as the stalled intermediate. Additional experiments involving solvent isotope effects, general base mutational analysis, and density functional calculations are consistent with impaired 2′-hydroxyl attack on the ADP-ribose-peptidyl intermediate. These results have implications for the development of mechanism-based inhibitors of Sir2 deacetylases.

Members of the silent information regulator 2 (Sir2 or sirtuin) family of protein deacetylases catalyze the conversion of acetyl-lysine residues and NAD^+ to deacetylated lysine, nicotinamide, and 2′-*O*-acetyl-ADP-ribose (*O*AADPr) (*1*, *2*). The most studied human Sir2 homologue, Sirt1, is reported to deacetylate a variety of substrates, including p53 (*3*−*5*), PPARγ (*6*), PGC-1α (*7*, *8*), and AceCS1 (*9*), implicating sirtuins in a broad range of biological processes, including stress resistance and glucose homeostasis. Sirtuin deacetylase activity has also been associated with pathways that oppose age-associated diseases, such as type II diabetes, obesity, and neurodegenerative disorders (*10*). The design of mechanism-based sirtuin inhibitors is aided by a detailed understanding of the chemical mechanism. Toward this end, it has been shown that sirtuins use a sequential mechanism in which the acetyl-lysine substrate binds first followed by NAD^+ to form a productive complex that undergoes catalysis in two main chemical steps (*11*). In the first portion of the proposed catalytic mechanism, the nicotinamide ribosyl bond of NAD^+ is cleaved and acetyl-lysine attacks to form nicotinamide and an α-1′-*O*-alkylamidate intermediate (*12*−*16*). In the second portion, an active site histidine activates the 2′-hydroxyl for attack of the *O*-alkylamidate to form a 1′,2′-cyclic intermediate (*15*). This is followed by addition of water to the 1′,2′-cyclic intermediate to form the product *O*AADPr and deacetylated peptide (*1*, *2*).

Recently, a thioacetyl-lysine peptide derived from the C-terminal region of p53 was shown to inhibit Sirt1-catalyzed deacetylation of an acetyl-lysine peptide with an IC_{50} value of 2 μM (*17*). The authors found the rate of Sirt1 de(thio)-acetylation with a thioacetyl p53 peptide was 400-fold slower than that of the corresponding acetyl-lysine peptide, though the cleavage of NAD^+ was suggested to be much less affected (*17*). Collectively, these observations suggested that this thioacetyl-lysine p53 peptide might form a catalytically less competent intermediate compared to an acetyl-lysine peptide. However, the mechanism of thioacetyl-lysine peptide inhibition and turnover by sirtuins was unknown. Here, we determine the chemical mechanism of thioacetyl-lysine peptide inhibition through mass spectrometry, pre-steady-state and steady-state kinetics, mutagenesis, isotope effects, and computational modeling.

EXPERIMENTAL PROCEDURES

Expression and Purification of His-Tagged Sir2 Homologues. Expression and purification of Hst2 (*1*, *13*), Hst2 H135A (*1*, *13*), Sirt1 (*9*, *18*), Sirt2 (*19*), and Sirt3 (*9*) were performed as previously described. The enzyme concentra-

[†] This work was supported by National Institutes of Health Grant GM065386 (to J.M.D.) and by National Institutes of Health Biotechnology Training Grant NIH 5 T32 GM08349 (to B.C.S.). Computational resources provided to the University of Wisconsin Chemistry Parallel Computing Center though NSF Grant CHE0091916 and gifts from Intel Corp.

* To whom correspondence should be addressed: Department of Biomolecular Chemistry, University of Wisconsin, 1300 University Ave., Madison, WI 53706-1532. Telephone: (608) 265-1859. Fax: (608) 262-5253. E-mail: jmdenu@wisc.edu.

[‡] Department of Chemistry.

[§] Department of Biomolecular Chemistry.

10.1021/bi7013294 CCC: $37.00
Published on Web 11/21/2007

tions were determined using the method of Bradford using BSA as the standard (*20*) unless otherwise stated. Enzyme aliquots were kept at −20 °C until they were used.

Solid-Phase Synthesis of Acetyl-Lysine Analogue Peptides. The acetyl, monofluoroacetyl, difluoroacetyl, and trifluoroacetyl peptides with the sequence NH_2-KSTGGK(ϵ-acetyl analogue)APRKQ-OH derivatized at the ϵ-amino group of the central lysine residue were synthesized according to previously published procedures (*21*). The thioacetyl-lysine peptide (ThioAcH3) was also synthesized in the same manner that was previously published using Fmoc-Lys($CSCH_3$)-OH (*17*). Thioacetyl-lysine peptide: MS (ESI) calcd for $C_{50}H_{91}N_{18}O_{15}S^+$ $[M + H]^+$ *m*/*z* 1215.7, found *m*/*z* 1215.9.

Isothermal Titration Calorimetry of Thioacetyl-Lysine Peptide Binding. The binding affinities of acetyl-lysine analogues for Hst2 were determined as previously described (*21*) using a VP-ITC instrument (MicroCal, Northampton, MA). Briefly, 0.22−0.4 μM thioacetyl-lysine peptide was injected into the cell containing 15−20 μM Hst2, and heats of binding were measured. Active enzyme concentrations were determined by measurement of the initial deacetylation rate using a [^{14}C]NAD^+/HPLC-based deacetylation assay (*22*) and compared to the previously published value of 0.2 s^{-1} (*13*). The least-squares fits to the binding parameters $\Delta H°$, K_d, and *N* were determined from the raw data using Origin (OriginLab, Northampton, MA).

Sir2 Homologue Inhibition by Thioacetyl-Lysine, Monofluoroacetyl-Lysine, Difluoroacetyl-Lysine, and Trifluoroacetyl-Lysine Peptides. Inhibition reactions were performed in 80 μL volumes containing 50 μM NAD^+, 20 μM [^{3}H]-acetyl-lysine peptide prepared as previously described (*19*), 1 mM DTT, 0.1−0.2 μM enzyme, and acetyl-lysine analogue peptide inhibitor concentrations ranging from 10 nM to 10 mM in 50 mM Tris (pH 7.5) at 25 °C. Reactions were initiated by addition of enzyme, mixtures incubated for 5−20 min, and reactions quenched with activated charcoal. Inhibition was assessed by measuring the initial forward rate of [^{3}H]*O*AADPr formation using the charcoal binding assay (*22*).

Dual-Reciprocal Inhibition Plots. Inhibition reactions were performed in 80 μL volumes containing 100 μM NAD^+, 2−32 μM [^{3}H]acetyl-lysine peptide (*19*), 1 mM DTT, 0.04 μM Hst2, and thioacetyl-lysine peptide concentrations ranging from 100 nM to 3 μM or trifluoroacetyl-lysine peptide concentrations ranging from 1 to 100 μM in 50 mM Tris (pH 7.5) at 25 °C. Reactions were initiated by addition of enzyme, mixtures incubated for 3−20 min, and reactions quenched with activated charcoal. Inhibition was assessed by measuring the initial forward rate of [^{3}H]*O*AADPr formation using the charcoal binding assay (*22*). The initial velocity data were fit in Kinetasyst (Intellikinetics, State College, PA) to competitive (eq 1 or 2) inhibition patterns based on the algorithms defined by Cleland (*23*). All data were displayed using Kaleidagraph (Synergy Software, Reading, PA).

$$v = \frac{V_{max}[S]}{K_m\left(1 + \frac{[I]}{K_{is}}\right) + [S]} \quad (1)$$

$$\log(v) = \log \frac{V_{max}[S]}{K_m\left(1 + \frac{[I]}{K_{is}}\right) + [S]} \quad (2)$$

Rapid-Quench Analysis of the Rate of Nicotinamide Formation. Single-turnover reactions were conducted with 325 μM [^{14}C]NAD^+, 15−20 μM thioacetyl-lysine peptide, 40 μM Hst2, and 1 mM DTT in 50 mM Tris-HCl (pH 7.5) at 25 °C. Time points from 28.5 to 4000 ms were assessed using a Hi-Tech RQF-63 rapid-quench flow system (TgK Scientific Ltd., Bradford on Avon, United Kingdom) and analyzed as previously described (*21*). In the rapid-quench flow, the contents of one syringe containing Hst2 and [^{14}C]-NAD^+ were rapidly mixed in a 1:1 ratio with the contents of another syringe containing thioacetyl-lysine peptide to obtain the final concentrations listed above. The concentration of nicotinamide formation was determined by scintillation counting of the HPLC fractions containing [^{14}C]-nicotinamide liberated from [^{14}C]NAD^+. To obtain the rate (*k*), the plot of product concentration formed over time was fitted to a single-exponential equation (eq 3)

$$P = [S]_0(1 - e^{-kt}) \quad (3)$$

where *P* is the concentration of product formed, $[S]_0$ is the initial concentration of the limiting substrate, and *t* is the reaction time.

Determination of the Catalytic Turnover Rate of Thioacetyl-Lysine Peptide with Hst2 and Hst2 H135A. A HPLC-based deacetylation assay using [^{14}C]NAD^+ was employed as previously described (*22*). The reactions were performed with 325 or 650 μM [^{14}C]NAD^+, 325 or 650 μM thioacetyl-lysine peptide, 1 mM DTT, and 6 μM Hst2 or Hst2 H135A in 50 mM Tris-HCl (pH 7.5) at 25 °C. Reactions were initiated by addition of enzyme and quenched with TFA at a final concentration of 1% (v/v). The rate of [^{14}C]-nicotinamide formation was determined by scintillation counting of the HPLC fractions corresponding to [^{14}C]-nicotinamide and [^{14}C]NAD^+. The rate of deacetylated peptide formation was determined by comparing peak areas of the deacetylated peptide and acetyl analogue peptide detected at 214 nm.

Identification of Products Formed by Thioacetyl-Lysine Peptide by Mass Spectrometry. Reactions conducted in 20 μL volumes containing 1 mM DTT, 400 μM thioacetyl-lysine peptide, 500 μM NAD^+, 50 μM Hst2 or Hst2 H135A, 0 or 20% (v/v) methanol, and 20 mM pyridine buffer adjusted to pH 7 with formic acid were reacted for 30−60 min at room temperature. Reaction mixtures were flash-frozen and stored at −20 °C until they were ready for mass spectral analysis as previously described (*15*).

Mass Spectrometry Detection of the Stalled Intermediate with Thioacetyl-Lysine Peptide. Reactions conducted in 20 μL volumes containing 1 mM DTT, 600 μM thioacetyl-lysine peptide, 500 μM NAD^+, 200 μM Hst2 or 150 μM Hst2 H135A, and 20 mM pyridine buffer adjusted to pH 7 with formic acid were reacted for 30−60 s at 25 °C. Controls were run in which thioacetyl-lysine peptide, NAD^+, or enzyme was removed from the reaction mixture. Reaction mixtures were flash-frozen and stored at −20 °C until they were ready for mass spectral analysis utilizing a Bruker

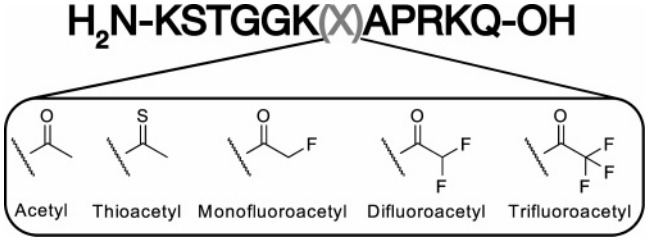

FIGURE 1: ϵ-Amino thioacetyl-lysine peptide (ThioAcH3), acetyl-lysine peptide (AcH3), and fluoroacetyl analogue peptides used in this study.

BIFLEX III matrix-assisted laser desorption ionization time-of-flight (MALDI-TOF) instrument in linear negative mode.

Solvent Isotope Effects with Acetyl- and Thioacetyl-Lysine Peptides. Dry buffer components were added directly to D_2O, and the pD was adjusted with DCl and NaOD. The pD values were determined by adding 0.4 to the reading of the pH electrode (*24*). Turnover rates were determined by measuring the rate of formation of [^{14}C]nicotinamide from [^{14}C]NAD$^+$ and the previously described HPLC assay (*22*). Reaction mixtures contained 1 mM DTT, 325 μM [^{14}C]NAD$^+$, 650 μM acetyl- or thioacetyl-lysine peptide, 50 mM Tris (pL 7.5) at 25 °C, and 2−6 μM Hst2. Reactions were initiated by addition of 4 μL of Hst2 (in H_2O) to a final volume of 160 μL. Time points were selected to measure after the initial burst of nicotinamide formation but before 10% conversion to products to ensure initial rate conditions.

Computational Methods. All calculations were performed with the Gaussian 03 package (*25*) using the three-parameter hybrid functional of Becke (*26*) together with the correlation functional of Lee, Yang, and Parr (*27*) (B3LYP) and the 6-31++G** basis set. Geometry optimizations were carried out on molecular fragments with methyl groups placed at the "cleavage sites" to prevent unwanted hydrogen bonding interactions. The cleavage sites were at the 5′-hydroxyl of the nicotinamide ribose of NAD$^+$ and the ϵ-carbon of the lysine side chain. To ensure optimized structures were true minima, vibrational frequencies were determined to check that no imaginary frequencies were present. Orbital energies were determined with natural bond order analysis, and orbital interaction energies were determined by second-order perturbation theory using NBO 5.G (*28*).

RESULTS AND DISCUSSION

Inhibition of Sirtuins by Histone H3 Peptide Containing Thioacetyl-Lysine. First, we examined whether thioacetyl-lysine peptide inhibition was a common feature among sirtuins. The IC_{50} values for human Sirt1, Sirt2, and Sirt3 and yeast Hst2 were measured using a synthesized thioacetyl-lysine peptide (ThioAcH3) as the inhibitor (Figure 1). This 11-mer peptide was based on the human histone H3 sequence modified at the ϵ-amino group of lysine 14 [H_2N-KSTGGK-(ϵ-thioacetyl)APRKQ-OH]. Indeed, similar inhibition was observed among the four Sir2 homologues, with IC_{50} values of 2.0 ± 0.2, 5.6 ± 0.8, 2.3 ± 0.3, and 1.02 ± 0.04 μM for Sirt1, Sirt2, Sirt3, and Hst2, respectively (Figure 2A). The result with Sirt1 was consistent with the previous report utilizing an ϵ-amino thioacetyl-lysine-containing p53 peptide (*17*).

Thioacetyl-Lysine Peptide Is a More Potent Inhibitor than Fluoroacetyl-Lysine Peptides. We have previously shown that monofluoroacetyl-, difluoroacetyl-, and trifluoroacetyl-lysine peptides (Figure 1) stall at the Michaelis complex with NAD$^+$ due to the decreased nucleophilicity of the acetyl oxygen (*21*). Therefore, we predicted that these fluoroacetyl-lysine peptides would be inhibitors of sirtuin deacetylation through competition for AcH3 at the Michaelis complex. To determine if ThioAcH3 inhibited by a similar mechanism, we compared the inhibition potency of ThioAcH3 to that of the fluoroacetyl-lysine peptides, employing Hst2 as the representative sirtuin (Figure 2B and Table 1). However, ThioAcH3 was by far the most potent inhibitor, with an IC_{50} >60-fold lower (1.0 μM vs ≥61 μM) than those of the three fluoroacetyl-lysine peptides that were tested.

To determine if this difference in inhibitor efficacy between ThioAcH3 and the fluoroacetyl-lysine peptides was simply a result of tighter binding of ThioAcH3, the K_d value for ThioAcH3 was measured and compared to those values previously determined with the fluoroacetyl-lysine peptides (*21*) (Table 1). Among the acetyl-lysine analogue peptides, the K_d values varied over an ~6-fold range from 3.3 to 21 μM. Interestingly, the ThioAcH3 and trifluoroacetyl-lysine peptide exhibited similar K_d values (4.7 and 3.3 μM, respectively) while having vastly different IC_{50} values (1.0 and 61 μM, respectively) (Table 1 and Figure 2B).

To compare the inhibition displayed by ThioAcH3 and trifluoroacetyl-lysine peptide directly to the K_d values, the K_i values for these peptides were obtained via steady-state inhibition analyses. Initial velocities for [^{3}H]*O*AADPr formation at saturating NAD$^+$ concentrations were determined at varied concentrations of [^{3}H]AcH3 as the substrate and either ThioAcH3 or trifluoroacetyl-lysine peptide as the inhibitor. At each inhibitor concentration, the data were plotted as 1/rate (v) versus 1/[AcH3], revealing a series of lines that intersected at the 1/v axis. Therefore, the inhibition was competitive with respect to AcH3, yielding K_{is} values (*29*) for ThioAcH3 and trifluoroacetyl-lysine peptide of 0.017 ± 0.003 and 4.8 ± 1.6 μM, respectively (Figure 3A). The K_{is} value (4.8 μM) for trifluoroacetyl-lysine peptide is similar to the K_d value of 3.3 μM (Figure 3B), consistent with inhibition occurring from competition with AcH3 for binding to free Hst2 and stalling at the Michaelis complex (*21*). However, the K_{is} value of 0.017 μM with ThioAcH3 was significantly below its K_d value of 4.7 μM, suggesting that ThioAcH3 inhibited primarily by stalling a reaction step after Michaelis complex formation.

Thioacetyl-Lysine Peptide as the Substrate Yields 1′-SH-OAADPr. To determine if ThioAcH3 was competent to proceed to the predicted product 1′-SH-2′-*O*-acetyl-ADP-ribose (1′-SH-*O*AADPr) (Scheme 1B) and therefore is processed by the equivalent dethioacetylation reaction as AcH3, we analyzed products formed from the NAD$^+$-dependent reaction of Hst2 with ThioAcH3. Using electrospray mass spectrometry in negative mode, we found that the enzyme-catalyzed dethioacetylation of ThioAcH3 produced 1′-SH-*O*AADPr, as revealed by a major peak at *m*/*z* 616.1 [calcd for $C_{17}H_{24}N_5O_{14}P_2S^-$ [M − H]$^-$ *m*/***z*** 616.1 (Figure 4)]. The small amount of *O*AADPr formed is likely due to hydrolysis of the 1′-thiol of 1′-SH-*O*AADPr during the course of the assay. These results indicated that Thio-

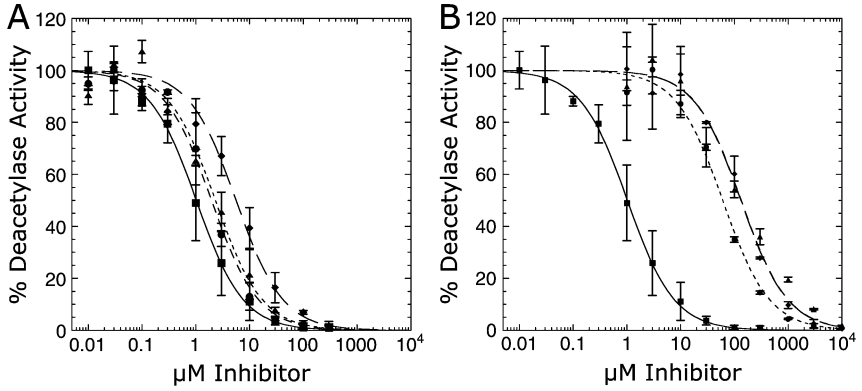

FIGURE 2: (A) Inhibition of the rate of acetyl-lysine deacetylation by ThioAcH3 of Hst2 (■), Sirt1 (●), Sirt2 (◆), and Sirt3 (▲). (B) Inhibition of Hst2 by ThioAcH3 (■), monofluoroacetyl-lysine peptide (▲), difluoroacetyl-lysine peptide (◆), and trifluoroacetyl-lysine peptide (●). Reaction mixtures contained 50 μM NAD^+, 20 μM [^{3}H]acetyl-lysine peptide, 1 mM DTT, 0.1−0.2 μM enzyme, and 10 nM to 10 mM acetyl-lysine analogue peptide inhibitor in 50 mM Tris (pH 7.5) at 25 °C. Inhibition was assessed by measuring the rate of [^{3}H]*O*AADPr formation using the charcoal binding assay (*22*). Error bars represent standard deviations from the mean.

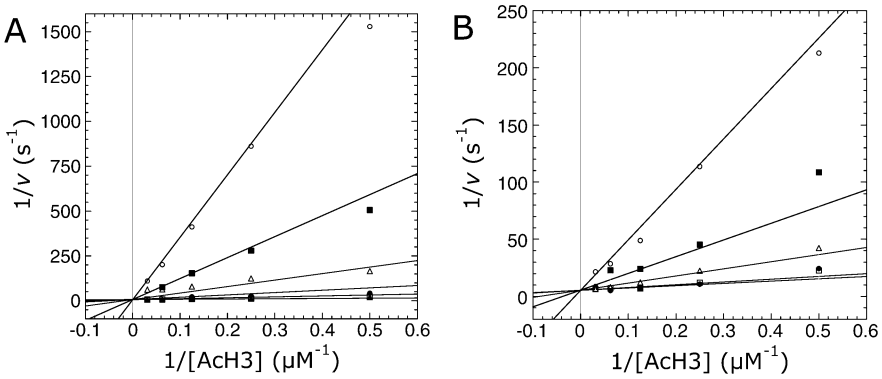

FIGURE 3: Double-reciprocal inhibition plots. Initial rates were determined from the rate of formation of [^{3}H]*O*AADPr from [^{3}H]AcH3 using the charcoal binding assay (*22*). The assay was performed in the presence of 100 μM NAD^+ and AcH3 concentrations ranging from 2 to 32 μM. (A) ThioAcH3 exhibits competitive inhibition toward AcH3 during the Hst2-catalyzed reaction. The following ThioAcH3 concentrations were used: 0 (▲), 0.03 (□), 0.1 (●), 0.3 (△), 1 (■), and 3 μM (○). (B) Trifluoroacetyl-lysine peptide exhibits competitive inhibition toward AcH3 during the Hst2-catalyzed reaction. The following trifluoroacetyl-lysine peptide concentrations were used: 0 (□), 1 (●), 10 (△), 30 (■), and 100 μM (○). Data were fit to competitive inhibition using KinetAsyst as described in Experimental Procedures.

Table 1: Physical and Kinetic Parameters of Acetyl-Lysine Analogues with Hst2

acetyl analogue peptide	nicotinamide formation (s^{-1})	k_{cat} (s^{-1})	K_d (μM)	$\Delta H°$ (kcal/mol)	N	IC_{50} (μM)	K_{is} (μM)
acetyl	$(6.7 \pm 0.9) \times 10^{0}$ [a]	$(2.0 \pm 0.3) \times 10^{-1}$[a]	21 ± 4[a]	-5.3 ± 3.9	0.96 ± 0.06	N/A[b]	N/A[b]
thioacetyl	$(4.5 \pm 0.9) \times 10^{0}$	$(2.4 \pm 0.1) \times 10^{-3}$	4.7 ± 1.0	-6.6 ± 3.7	1.07 ± 0.24	1.02 ± 0.04	0.017 ± 0.003
monofluoroacetyl	$(3.7 \pm 0.6) \times 10^{-3}$[a]	$(3.3 \pm 0.5) \times 10^{-3}$[a]	22 ± 5[a]	-4.5 ± 1.9	1.02 ± 0.02	133 ± 21	N/A[b]
difluoroacetyl	$(4.6 \pm 0.8) \times 10^{-5}$[a]	N/A[b]	20 ± 1[a]	-10.3 ± 2.1	1.04 ± 0.20	132 ± 12	N/A[b]
trifluoroacetyl	$(1.1 \pm 0.4) \times 10^{-5}$[a]	N/A[b]	3.3 ± 0.7[a]	-9.0 ± 1.3	0.99 ± 0.07	61 ± 6	4.8 ± 1.6

[a] Data from ref *21*. [b] Not available.

AcH3 could be turned over to yield products analogous to those with acetyl-lysine peptides and suggest that inhibition might be due to formation of a stalled catalytic intermediate rather than a dead-end complex.

Thioacetyl-Lysine Peptide Displays Slow Overall Turnover Rates. To examine the possibility that ThioAcH3 stalls the enzyme at an intermediate along the catalytic pathway, a series of steady-state and pre-steady-state rapid-quenching kinetic analyses were performed. Catalytic stalling with ThioAcH3 predicts a significant retardation of the overall turnover rate (k_{cat}) compared to the value of 0.2 s^{-1} with AcH3 (*21*). Indeed, measurement of the steady-state rate of nicotinamide formation at saturating NAD^+ and ThioAcH3 concentrations resulted in a turnover rate (k_{cat}) of $(2.4 \pm 0.1) \times 10^{-3}$ s^{-1}, which is ~80-fold slower than the rate using AcH3 (Table 1). A similar steady-state rate of $(2.1 \pm 0.7) \times 10^{-3}$ s^{-1} was determined from dethioacetylated peptide formation. This suggested that the 1:1 stoichiometry of NAD^+ cleavage to deacetylation is retained when using ThioAcH3 and that ThioAcH3 is processed by the same mechanism as AcH3, albeit with an extremely low efficiency.

Thioacetyl-Lysine Peptide Displays Rapid Nicotinamide Formation. To resolve the step in catalysis that is altered with ThioAcH3 as a substrate, the rate of nicotinamide formation was measured under rapid single-turnover conditions. Using ThioAcH3, a first-order rate of 4.5 ± 0.9 s^{-1} for nicotinamide formation was determined, similar to the previously published value of 6.7 ± 0.9 s^{-1} (*21*) for AcH3 (Figure 5 and Table 1). A similar pre-steady-state rate for nicotinamide formation suggested that ThioAcH3 was readily converted to the predicted 1′-*S*-alkylamidate intermediate, but that a subsequent step was impeded, as shown by an

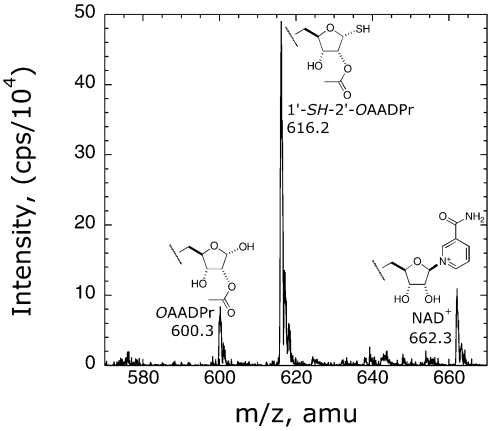

FIGURE 4: Detection of products formed with ThioAcH3 and Hst2 by electrospray mass spectrometry in negative mode. Reaction mixtures contained 1 mM DTT, 400 μM ThioAcH3, 500 μM NAD^+, 50 μM Hst2, and 20 mM pyridine buffer adjusted to pH 7 with formic acid.

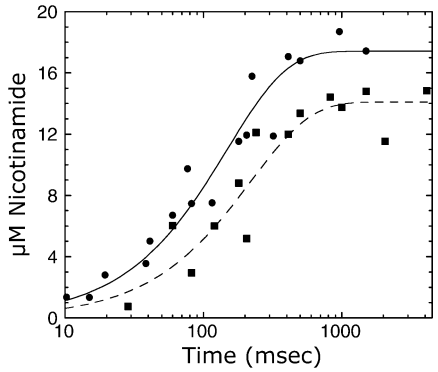

FIGURE 5: Rapid-quench flow analysis of AcH3 (●) and ThioAcH3 (■) as substrates. Single-turnover reactions were conducted with 325 μM [^{14}C]NAD^+, 15−20 μM ThioAcH3 or AcH3, 40 μM Hst2, and 1 mM DTT in 50 mM Tris (pH 7.5) at 25 °C. Time points from 10.3 to 4000 ms were evaluated using a Hi-Tech RQF-63 rapid-quench flow system and analyzed as previously described (*21*). To obtain the rate (k), the plot of product concentration formed over time was fitted to the single-exponential equation [$P = [S]_0(1 - e^{-kt})$]. Points for acetyl-lysine were published previously (*21*).

~2000-fold slower rate of turnover (k_{cat}) compared to the rate of nicotinamide formation under single-turnover conditions.

Kinetic Modeling of Inhibition. To explain the effects of reaction kinetics on the distinct inhibitory behavior of the ThioAcH3 and trifluoroacetyl-lysine peptides, we used steady-state kinetic modeling and applied the equilibrium and rate constants determined from the various kinetic and equilibrium experiments. Sirtuins employ a sequential kinetic mechanism in which the acetyl-lysine substrate binds first followed by NAD^+ to form the Michaelis complex. This complex then reacts, resulting in nicotinamide and the alkylamidate intermediate. Nicotinamide is released, and the alkylamidate is further processed to yield deacetylated peptide and *O*AADPr (*11*). At saturating NAD^+ concentrations, the kinetic mechanism can be simplified into three main steps: initial acetyl-lysine substrate binding, reaction to form nicotinamide, and final formation of deacetylated peptide and *O*AADPr. Under initial velocity conditions, the release of all products is irreversible, so only the forward rate constants are shown (Figure 6). Using the net rate constant method of Cleland (*30*), the inhibition constant K_{is} (*29*) can be expressed in terms of the individual kinetic constants for this simplified mechanism (Figure 6) as shown below:

$$K_{is} = \frac{k_8k_{11} + k_9k_{11}}{k_7k_{11} + k_7k_9} = \frac{K_dk_7k_{11} + k_9k_{11}}{k_7k_{11} + k_7k_9} = K_d\left(\frac{k_8k_{11} + k_9k_{11}}{k_8k_{11} + k_8k_9}\right)$$

In the case of ThioAcH3, the pre-steady-state rate of nicotinamide formation ($k_9 = 4.5\ s^{-1}$) is much faster than the steady-state turnover rate ($k_{cat} = k_{11} = 0.0024\ s^{-1}$). Therefore, the above equation can be simplified to

$$K_{is} = \frac{k_8k_{cat} + k_9k_{cat}}{k_7k_9} = K_m \quad \text{where} \quad \frac{k_{cat}}{K_m} = \frac{k_{11}}{K_m} = \frac{k_7k_9}{k_8 + k_9}$$

Therefore, the observed K_{is} for ThioAcH3 is equal to its K_m as an alternative substrate. We can estimate k_7 or k_8 for ThioAcH3 using previously published values with AcH3 for the nicotinamide formation rate (6.7 s^{-1}), k_{cat} (0.24 s^{-1}), K_m (4.3 μM), and K_d (21 μM) (*11*, *21*). Using this method, we calculate limiting k_7 and k_8 values for ThioAcH3 of $\geq 6.8 \times 10^4\ s^{-1}\ M^{-1}$ and $\leq 1.4\ s^{-1}$, respectively. As the lower K_d value displayed by ThioAcH3 compared to that of AcH3 might be due to both a small decrease in the rate of dissociation (k_8) and a small increase in the rate of association (k_7), substitution of only one of these calculated k_7 or k_8 values into the above equations provides limiting cases of 10 and 38 nM on the predicted K_{is} value. Indeed, the measured K_{is} value of 17 nM for ThioAcH3 falls between these two limits. Thus, this potent inhibition is entirely consistent with stalling at an intermediate enzyme form in which substrate AcH3 cannot compete. Competitive inhibition patterns are observed since infinite AcH3 concentrations would keep finite concentrations of ThioAcH3 from binding to free enzyme.

In the case of trifluoroacetyl-lysine peptide, the rate of nicotinamide formation is very slow compared to the other rate constants ($k_9 \ll k_8$ or k_{11}). Therefore, the trifluoroacetyl-lysine peptide is predicted to exhibit a K_{is} value near its K_d since, when k_9 is very small, the formula above for K_{is} reduces to $K_{is} = K_d$. Indeed, we determined a K_{is} value of 4.8 μM for trifluoroacetyl-lysine peptide, similar to its K_d value of 3.3 μM.

Detection of an ADP-Ribose−Peptide Intermediate with Thioacetyl-Lysine Peptide. To gain insight into the nature of the stalled intermediate, we analyzed potential novel species formed during the Hst2-catalyzed dethioacetylation of ThioAcH3. To minimize the manipulation required prior to analysis, the mass spectrometry samples were taken directly from unquenched reactions. Using MALDI-TOF MS, we identified a unique species at *m*/*z* 1754.3, which was dependent on the presence of Hst2, ThioAcH3, and NAD^+, indicating this new species was a result of Hst2-catalyzed reaction with ThioAcH3 and NAD^+ (Figure 7A−D). This new peak at *m*/*z* 1754.3 was consistent with the mass expected for either a stalled 1′-*S*-alkylamidate, the subsequent 1′,2′-cyclic thioalkyl intermediate along the proposed catalytic pathway, or another isomer not on the proposed catalytic pathway (Scheme 1B). As discussed below, additional results

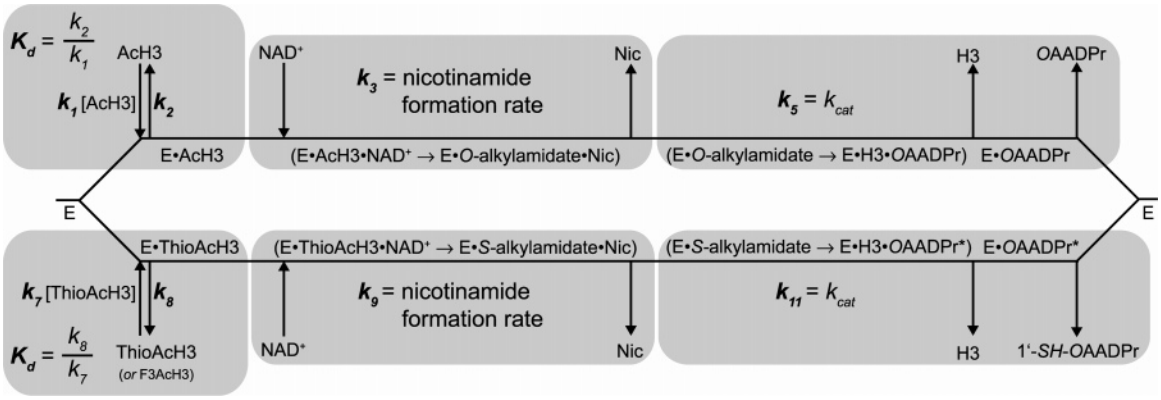

FIGURE 6: Proposed kinetic mechanism of ThioAcH3 alternate substrate inhibition of sirtuin-catalyzed AcH3 deacetylation.

Scheme 1: Proposed Chemical Mechanism of (A) Acetyl-Lysine (AcH3) and (B) Thioacetyl-Lysine Peptide (ThioAcH3) Substrates

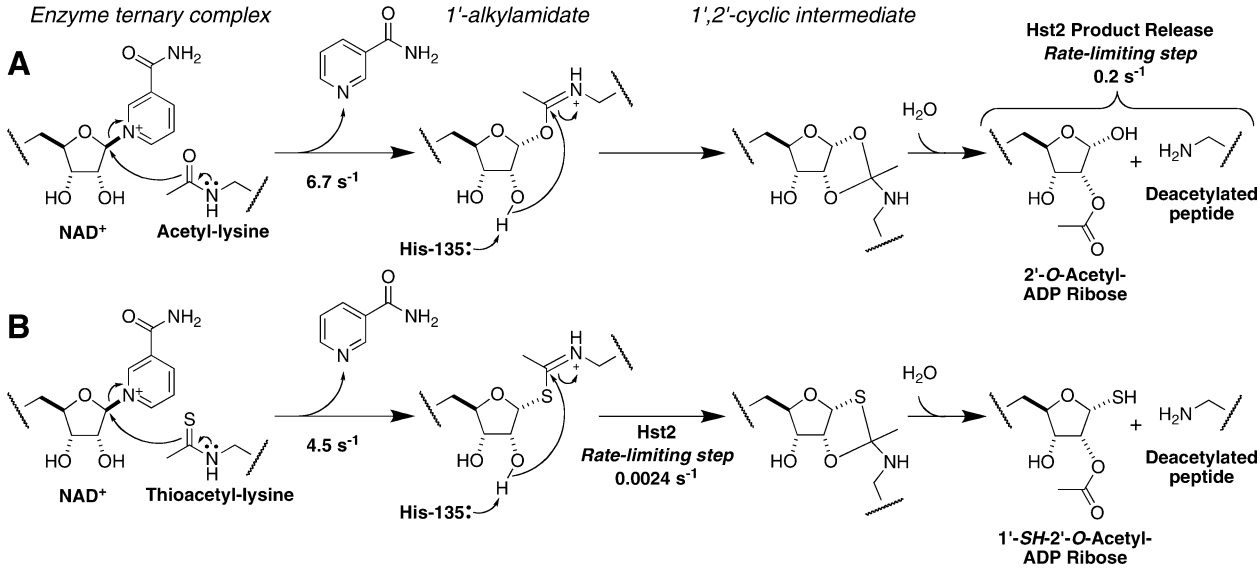

are most consistent with the species at *m*/*z* 1754.3 being the 1′-*S*-alkylamidate.

Mutation of Histidine 135 to Alanine Further Slows Dethioacetylation. To help distinguish between stalling at the 1′-*S*-alkylamidate versus the 1′,2′-cyclic intermediate, we utilized a Hst2 mutant enzyme (Hst2 H135A) in which the active site histidine is mutated to alanine. His135 is responsible for general base activation of the 2′-hydroxyl for attack of the 1′-alkylamidate to form the 1′,2′-cyclic intermediate (*15*) (Scheme 1). Previously, we have shown that mutation of this histidine decreased the rate of deacetylation (k_{cat}) of AcH3 approximately 20-fold from ∼0.2 to ∼0.01 s^{-1} at pH 7.5 (*15*). However, mutation of this histidine minimally affected the cleavage of NAD^+ in forming the 1′-alkylamidate as shown by a small 3-fold reduction in nicotinamide transglycosidation rate with AcH3 (*13*). If 2′-hydroxyl attack of the 1′-*S*-alkylamidate were rate-limiting, then a multiplicative reduction in the steady-state deacetylation rate would be predicted when utilizing ThioAcH3 with Hst2 H135A. Because the steady-state rate with wild-type Hst2 is reduced ∼100-fold with ThioAcH3 compared to AcH3, we predict a rate reduction of ∼2000-fold (∼1×10^{-4} s^{-1}) when using ThioAcH3 and Hst2 H135A together. Indeed, we found a rate of ≤5×10^{-4} s^{-1} with ThioAcH3 and Hst2 H135A, consistent with an additional attenuation of the ability of the enzyme to proceed beyond the 1′-*S*-alkylamidate. Furthermore, mass spectral analysis of the Hst2 H135A-catalyzed reaction of ThioAcH3 revealed a species corresponding to deacetylated peptide and the 1′-*S*-alkylamidate intermediate (Figure 7E), suggesting that the mutant enzyme is not significantly impeded up to formation of the 1′-*S*-alkylamidate and does proceed to dethioacetylation, albeit at a much slower rate.

Thioacetyl-Lysine Peptide Displays a Large Solvent Isotope Effect. If the sirtuin-catalyzed reaction with ThioAcH3 were stalled at the 1′-*S*-alkylamidate, this rate-limiting step would be expected to yield a significant normal solvent isotope effect for ThioAcH3, as proton abstraction by the general base histidine of the ribose 2′-hydroxyl is critical for attack on the 1′-*S*-alkylamidate. Indeed, reaction of ThioAcH3 revealed a large solvent isotope effect of 4.1 ± 0.6 on the V_{max} value, consistent with stalling at the 1′-*S*-alkylamidate. In contrast, AcH3 exhibited an only modest solvent isotope effect of 1.6 ± 0.2. It was previously shown that the reaction rates of AcH3 with Hst2 correlate with solution viscosity due to a rate-limiting product release step (*15*). Therefore, a significant portion of the small isotope effect observed for AcH3 can be explained by the increased viscosity of D_2O versus H_2O [1.100 mPa s vs 0.8903 mPa s; ratio of 1.24 at 25 °C (*39*)].

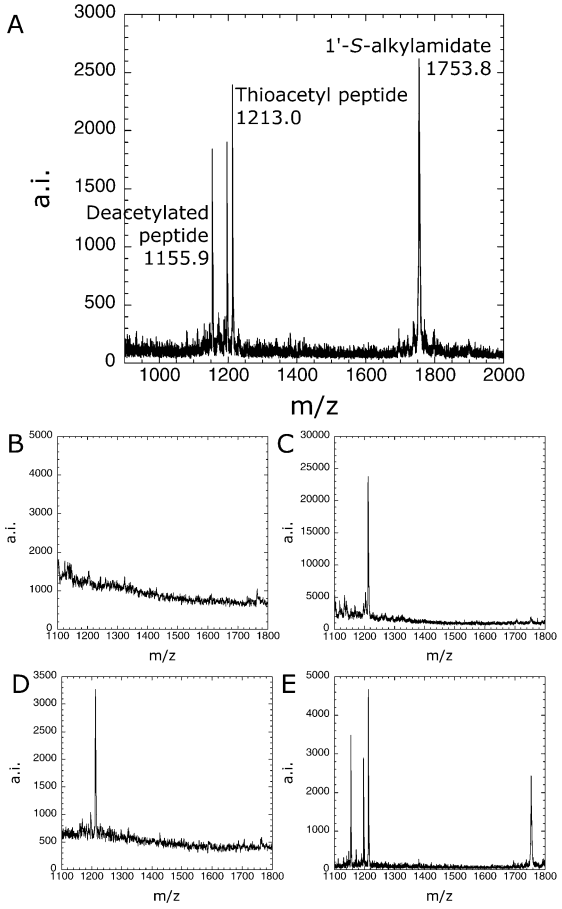

FIGURE 7: Mass spectrometry detection of 1′-*S*-alkylamidate with ThioAcH3. Spectra shown are from (A) the reaction mixture containing 1 mM DTT, 600 μM ThioAcH3, 500 μM NAD^+, 200 μM Hst2 WT, and 20 mM pyridine formate buffer, (B) the reaction mixture without ThioAcH3, (C) the reaction mixture without enzyme, (D) the reaction mixture without NAD^+, and (E) the reaction mixture with Hst2 H135A instead of Hst2 WT.

Computational and Chemical Modeling Support Inefficient Attack of the 2′-Hydroxyl at the 1′-S-Alkylamidate. One possible explanation for a decreased rate of 2′-hydroxyl attack at the 1′-*S*-alkylamidate compared to that at the 1′-*O*-alkylamidate is that the 2′-hydroxyl is not positioned optimally for nucleophilic attack in the 1′-*S*-alkylamidate. To examine this possibility, computational studies were performed. Initially utilizing the coordinates of the ribose ring and acetyl-lysine from the X-ray structure of NAD^+ and acetyl-lysine peptide bound to Sir2Tm (*12*), the geometries of fragments of the 1′-*O*-alkylamidate and 1′-*S*-alkylamidate were optimized. In these models, interactions with protein residues are removed for computational simplicity since the enzymatic environment is predicted to be unchanged when using an alternate substrate with a single-atom substitution. This optimization revealed distances of 2.97 and 3.36 Å between the 2′-oxygen and the imidate carbon for the 1′-*O*-alkylamidate and 1′-*S*-alkylamidate, respectively (Figure 8). The longer distance within the 1′-*S*-alkylamidate is consistent with a slower attack of the 2′-hydroxyl within this intermediate. Geometry optimization also revealed angles among the 2′-oxygen, imidate carbon, and imidate nitrogen of 122° and 138° for the 1′-*O*-alkylamidate and 1′-*S*-alkylamidate, respectively (Figure 8). The Bürgi−Dunitz trajectory predicts an optimal angle of ~110° for an oxygen nucleophile

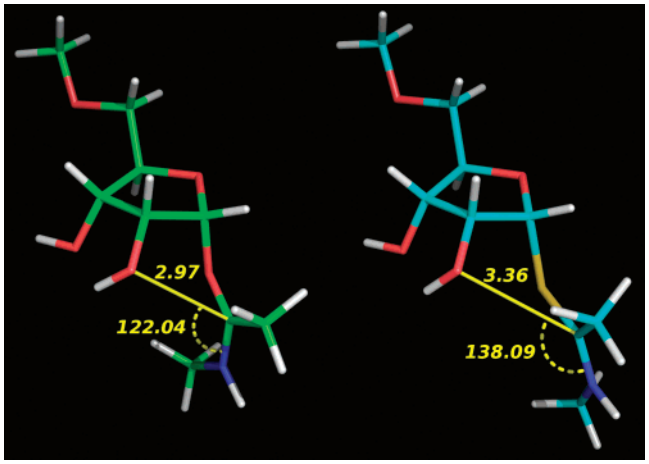

FIGURE 8: Geometry-optimized conformations of the fragment of (left) 1′-*O*-alkylamidate and (right) 1′-*S*-alkylamidate. Shown are the distances from the 2′-oxygen to the imidate carbon in angstroms and the angle among the 2′-oxygen, imidate carbon, and imidate nitrogen in degrees. Calculations were performed with Gaussian 03 (*25*) using the three-parameter hybrid functional B3LYP and the 6-31++G** basis set.

approaching a carbonyl group in an acyl transfer reaction (*31*−*33*). This trajectory results from maximal overlap between the lone pair (n) of the oxygen nucleophile and the antibonding orbital (π^*) of the carbonyl group while minimizing steric effects. Therefore, the angle of attack in the 1′-*O*-alkylamidate is closer to the ideal angle compared to that in the 1′-*S*-alkylamidate, predicting a faster rate of 2′-hydroxyl attack with the 1′-*O*-alkylamidate. Additionally, natural bond order analysis (*28*) indicated a 1.31 kcal/mol n $\rightarrow \pi^*$ interaction in which electron density of a lone pair on the 2′-oxygen is donated to the antibonding orbital of the imidate carbon−nitrogen bond for the 1′-*O*-alkylamidate. This interaction is important since these orbitals form the new bond in the 1′,2′-cyclic intermediate. However, this interaction is <0.5 kcal/mol in the 1′-*S*-alkylamidate, further slowing the reaction with the 1′-*S*-alkylamidate. These altered bond angles and distances within the 1′-*S*-alkylamidate compared to the 1′-*O*-alkylamidate may also reposition the 2′-hydroxyl relative to the active site general base histidine. This repositioning could weaken the activation of the 2′-hydroxyl by the active site histidine, thereby slowing the rate of 2′-hydroxyl attack in the 1′-*S*-alkylamidate.

Another possible explanation for slowed 2′-hydroxyl attack is that the pK_a value of the imidate nitrogen is lowered in the 1′-*S*-alkylamidate, which would impede the rate of 2′-hydroxyl attack since nucleophilic attack on the imidate carbon requires a protonated imidate nitrogen (*34*, *35*). However, hydrolysis of *N*-alkyl acetimidate esters (*36*, *37*) or *N*-alkyl thioacetimidate esters (*34*, *35*) in chemical model systems predicts pK_a values of the 1′-*O*-alkylamidate and 1′-*S*-alkylamidate of ~7.5 and ~7.75, respectively. These intrinsic pK_a values are not significantly different and therefore are not sufficient to explain the variation in reactivity between the two intermediates. Nonetheless, we cannot rule out the possibility that the change in bond lengths and angles within the 1′-*S*-alkylamidate places the imidate nitrogen in a different local environment, which could alter the pK_a value and therefore the reactivity.

A third explanation for a slowed rate of 2′-hydroxyl attack in the 1′-*S*-alkylamidate is that the reactivity of the imidate

carbon is inherently lower in the 1′-*S*-alkylamidate than in the 1′-*O*-alkylamidate. Indeed, chemical model studies show an ~3−4 fold slower rate of hydrolysis for *N*-alkyl thioacetimidate esters versus *N*-alkyl acetimidate esters (~1.6−1.8 × 10^{-5} s^{-1} vs 5.1−6.7 × 10^{-5} s^{-1}) (*34*−*37*), indicating that the imidate carbon in the 1′-*S*-alkylamidate is a weaker electrophile than the 1′-*O*-alkylamidate. Therefore, both the inherent reactivity of the 1′-*S*-alkylamidate and the relative positioning of the 2′-hydroxyl support a slower rate of 2′-hydroxyl attack in the 1′-*S*-alkylamidate compared to the 1′-*O*-alkylamidate, consistent with the Hst2-catalyzed dethioacetylation reaction stalling at the 1′-*S*-alkylamidate.

CONCLUSIONS

We provide evidence that thioacetyl-lysine peptides exhibit mechanism-based inhibition of sirtuins primarily by stalling an enzyme intermediate. This inhibitory mechanism is in stark contrast to the fluoroacetyl-lysine peptides that inhibit sirtuin deacetylation through competition for acetyl-lysine peptide binding to free enzyme but are prevented from undergoing significant catalysis. While we cannot completely rule out other possibilities, the collective data for thioacetyl-lysine peptide are most consistent with stalling at the 1′-*S*-alkylamidate intermediate. This study provides a groundwork for the development of a variety of chemical tools for further studying the biology of sirtuin protein deacetylases. The mechanism-based inhibition of sirtuins displayed by thioacetyl-lysine peptides will be invaluable in the further rational design of mechanism-based inhibitors and activity-based probes of Sir2 deacetylases. In particular, yet undiscovered alternative substrates that undergo more rapid NAD^+ cleavage in the first step or slower formation of products (or formation of a dead-end intermediate that does not turnover) compared to ThioAcH3 would be predicted to exhibit even greater sirtuin inhibition. Furthermore, attachment of a fluorophore and photolabeling group to these chemical probes could allow synthesis of activity-based probes (*38*), providing a direct readout for sirtuin activity in cell extracts and perhaps live cells. Alternatively, attachment of a photolabeling group might label other associated proteins, providing a method of identifying sirtuin protein complexes. Also, insertion of the thioacetyl-lysine "war-head" into peptide sequences that are specific substrates for a given sirtuin may allow for the facile discovery of selective sirtuin inhibitors. These new chemical tools will be useful in elucidating the roles of protein deacetylases in a variety of human disease states such as cancer, diabetes, and neurodegeneration.

ACKNOWLEDGMENT

We thank Ronald Raines, Laura Kiessling, W. Wallace Cleland, and members of the Denu group, especially Chris Berndsen, for valuable discussions. We also thank Dr. Gary Case for assistance with the peptide syntheses, Dr. Amy Harms for assistance with the mass spectrometry experiments, and Dr. Hieu Tran for assistance with the computational experiments.

REFERENCES

1. Jackson, M. D., and Denu, J. M. (2002) Structural identification of 2′- and 3′-O-acetyl-ADP-ribose as novel metabolites derived from the Sir2 family of β-NAD^+-dependent histone/protein deacetylases, *J. Biol. Chem. 277*, 18535−18544.
2. Sauve, A. A., Celic, I., Avalos, J., Deng, H., Boeke, J. D., and Schramm, V. L. (2001) Chemistry of gene silencing: The mechanism of NAD^+-dependent deacetylation reactions, *Biochemistry 40*, 15456−15463.
3. Luo, J., Nikolaev, A. Y., Imai, S., Chen, D., Su, F., Shiloh, A., Guarente, L., and Gu, W. (2001) Negative control of p53 by Sir2α promotes cell survival under stress, *Cell 107*, 137−148.
4. Vaziri, H., Dessain, S. K., Ng Eaton, E., Imai, S. I., Frye, R. A., Pandita, T. K., Guarente, L., and Weinberg, R. A. (2001) hSIR2-(SIRT1) functions as an NAD-dependent p53 deacetylase, *Cell 107*, 149−159.
5. Langley, E., Pearson, M., Faretta, M., Bauer, U. M., Frye, R. A., Minucci, S., Pelicci, P. G., and Kouzarides, T. (2002) Human SIR2 deacetylates p53 and antagonizes PML/p53-induced cellular senescence, *EMBO J. 21*, 2383−2396.
6. Picard, F., Kurtev, M., Chung, N., Topark-Ngarm, A., Senawong, T., Machado, De Oliveira, R., Leid, M., McBurney, M. W., and Guarente, L. (2004) Sirt1 promotes fat mobilization in white adipocytes by repressing PPAR-γ, *Nature 429*, 771−776.
7. Nemoto, S., Fergusson, M. M., and Finkel, T. (2005) SIRT1 functionally interacts with the metabolic regulator and transcriptional coactivator PGC-1α, *J. Biol. Chem. 280*, 16456−16460.
8. Rodgers, J. T., Lerin, C., Haas, W., Gygi, S. P., Spiegelman, B. M., and Puigserver, P. (2005) Nutrient control of glucose homeostasis through a complex of PGC-1α and SIRT1, *Nature 434*, 113−118.
9. Hallows, W. C., Lee, S., and Denu, J. M. (2006) Sirtuins deacetylate and activate mammalian acetyl-CoA synthetases, *Proc. Natl. Acad. Sci. U.S.A. 103*, 10230−10235.
10. Haigis, M. C., and Guarente, L. P. (2006) Mammalian sirtuins: Emerging roles in physiology, aging, and calorie restriction, *Genes Dev. 20*, 2913−2921.
11. Borra, M. T., Langer, M. R., Slama, J. T., and Denu, J. M. (2004) Substrate specificity and kinetic mechanism of the Sir2 family of NAD^+-dependent histone/protein deacetylases, *Biochemistry 43*, 9877−9887.
12. Hoff, K. G., Avalos, J. L., Sens, K., and Wolberger, C. (2006) Insights into the sirtuin mechanism from ternary complexes containing NAD^+ and acetylated peptide, *Structure 14*, 1231−1240.
13. Jackson, M. D., Schmidt, M. T., Oppenheimer, N. J., and Denu, J. M. (2003) Mechanism of nicotinamide inhibition and transglycosidation by Sir2 histone/protein deacetylases, *J. Biol. Chem. 278*, 50985−50998.
14. Sauve, A. A., and Schramm, V. L. (2003) Sir2 regulation by nicotinamide results from switching between base exchange and deacetylation chemistry, *Biochemistry 42*, 9249−9256.
15. Smith, B. C., and Denu, J. M. (2006) Sir2 protein deacetylases: Evidence for chemical intermediates and functions of a conserved histidine, *Biochemistry 45*, 272−282.
16. Zhao, K., Harshaw, R., Chai, X., and Marmorstein, R. (2004) Structural basis for nicotinamide cleavage and ADP-ribose transfer by NAD^+-dependent Sir2 histone/protein deacetylases, *Proc. Natl. Acad. Sci. U.S.A. 101*, 8563−8568.
17. Fatkins, D. G., Monnot, A. D., and Zheng, W. (2006) Nepsilon-thioacetyl-lysine: A multi-facet functional probe for enzymatic protein lysine Nϵ-deacetylation, *Bioorg. Med. Chem. Lett. 16*, 3651−3656.
18. Borra, M. T., Smith, B. C., and Denu, J. M. (2005) Mechanism of human SIRT1 activation by resveratrol, *J. Biol. Chem. 280*, 17187−17195.
19. Borra, M. T., O'Neill, F. J., Jackson, M. D., Marshall, B., Verdin, E., Foltz, K. R., and Denu, J. M. (2002) Conserved enzymatic production and biological effect of O-acetyl-ADP-ribose by silent information regulator 2-like NAD^+-dependent deacetylases, *J. Biol. Chem. 277*, 12632−12641.
20. Bradford, M. M. (1976) A rapid and sensitive method for the quantitation of microgram quantities of protein utilizing the principle of protein-dye binding, *Anal. Biochem. 72*, 248−254.
21. Smith, B. C., and Denu, J. M. (2007) Sir2 deacetylases exhibit nucleophilic participation of acetyl-lysine in NAD^+ cleavage, *J. Am. Chem. Soc. 129*, 5802−5803.
22. Borra, M. T., and Denu, J. M. (2004) Quantitative assays for characterization of the Sir2 family of NAD^+-dependent deacetylases, *Methods Enzymol. 376*, 171−187.
23. Cleland, W. W. (1977) Determining the chemical mechanisms of enzyme-catalyzed reactions by kinetic studies, *Adv. Enzymol. Relat. Areas Mol. Biol. 45*, 273−387.

24. Schowen, K. B., and Schowen, R. L. (1982) Solvent isotope effects of enzyme systems, *Methods Enzymol. 87*, 551−606.
25. Frisch, M. J., Trucks, G. W., Schlegel, H. B., Scuseria, G. E., Robb, M. A., Cheeseman, J. R., Montgomery, J. A., Jr., Vreven, T., Kudin, K. N., Burant, J. C., Millam, J. M., Iyengar, S. S., Tomasi, J., Barone, V. B. M., Cossi, M., Scalmani, G., Rega, N., Petersson, G. A., Nakatsuji, H., Hada, M., Ehara, M., Toyota, K., Fukuda, R. J. H., Ishida, M., Nakajima, T., Honda, Y., Kitao, O., Nakai, H., Klene, M., Li, X., Knox, J. E., Hratchian, H. P., Cross, J. B., Adamo, C., Jaramillo, J., Gomperts, R., Stratmann, R. E., Yazyev, O., Austin, A. J., Cammi, R., Pomelli, C., Ochterski, J. W., Ayala, P. Y., Morokuma, K., Voth, G. A., Salvador, P., Dannenberg, J. J., Zakrzewski, V. G., Dapprich, S., Daniels, A. D., Strain, M. C., Farkas, O., Malick, D. K., Rabuck, A. D., Raghavachari, K., Foresman, J. B., Ortiz, J. V., Cui, Q., Baboul, A. G., Clifford, S., Cioslowski, J., Stefanov, B. B., Liu, G., Liashenko, A., Piskorz, P., Komaromi, I., Martin, R. L., Fox, D. J., Keith, T., Al-Laham, M. A., Peng, C. Y., Nanayakkara, A., Challacombe, M., Gill, P. M. W., Johnson, B., Chen, W., Wong, M. W., Gonzalez, C., and Pople, J. A. (2003) *Gaussian 03*, Gaussian, Inc., Pittsburgh, PA.
26. Becke, A. D. (1988) Density-functional exchange-energy approximation with correct asymptotic behavior, *Phys. Rev. A: At., Mol., Opt. Phys. 38*, 3098−3100.
27. Lee, C., Yang, W., and Parr, R. G. (1988) Development of the Colle-Salvetti correlation-energy formula into a functional of the electron density, *Phys. Rev. B: Condens. Matter Mater. Phys. 37*, 785−789.
28. Glendening, E. D., Badenhoop, J. K., Reed, A. E., Carpenter, J. E., Bohmann, J. A., Morales, C. M., and Weinhold, F. (2001) *NBO 5.G*, Theoretical Chemistry Institute, University of Wisconsin, Madison, WI.
29. Segel, I. H. (1975) *Enzyme kinetics: Behavior and analysis of rapid equilibrium and steady-state enzyme systems*, 1993 ed., Wiley-Interscience, New York.
30. Cleland, W. W. (1975) Partition analysis and concept of net rate constants as tools in enzyme kinetics, *Biochemistry 14*, 3220−3224.
31. Bürgi, H. B., Dunitz, J. D., Lehn, J. M., and Wipff, G. (1974) Stereochemistry of reaction paths at carbonyl centers, *Tetrahedron 30*, 1563−1572.
32. Bürgi, H. B., Dunitz, J. D., and Shefter, E. (1974) Chemical reaction paths. IV. O···C═O interactions in crystals, *Acta Crystallogr. B30* (Part 6), 1517−1527.
33. Bürgi, H. B., Dunitz, J. D., and Shefter, E. (1973) Geometrical reaction coordinates. II. Nucleophilic addition to a carbonyl group, *J. Am. Chem. Soc. 95*, 5065−5067.
34. Chaturvedi, R. K., MacMahon, A. E., and Schmir, G. L. (1967) Hydrolysis of thioimidate esters. Tetrahedral intermediates and general acid catalysis, *J. Am. Chem. Soc. 89*, 6984−6993.
35. Chaturvedi, R. K., and Schmir, G. L. (1969) Hydrolysis of thioimidate esters. II. Evidence for the formation of three species of the tetrahedral intermediate, *J. Am. Chem. Soc. 91*, 737−746.
36. Chaturvedi, R. K., and Schmir, G. L. (1968) The hydrolysis of N-substituted acetimidate esters, *J. Am. Chem. Soc. 90*, 4413−4420.
37. Pletcher, T. C., Koehler, S., and Cordes, E. H. (1968) Mechanism of hydrolysis of N-methylacetimidate esters, *J. Am. Chem. Soc. 90*, 7072−7076.
38. Jessani, N., and Cravatt, B. F. (2004) The development and application of methods for activity-based protein profiling, *Curr. Opin. Chem. Biol. 8*, 54−59.
39. Cho, C. H., Urquidi, J., Singh, S., and Robinson, G. W. (1999) Thermal Offset Viscosities of Liquid H_2O, D_2O, and T_2O, *J. Phys. Chem. B 103*, 1991−1994.

BI7013294